On the possibility to detect multipolar order in URu$_2$Si$_2$ by the electric quadrupolar transition of resonant elastic x-ray scattering

Y. L. Wang,[1] G. Fabbris,[1] D. Meyers,[1] N. H. Sung,[2] R. E. Baumbach,[2,3] E. D. Bauer,[2] P. J. Ryan,[4,5]
J.-W. Kim,[4] X. Liu,[6] M. P. M. Dean,[1] G. Kotliar,[1,7] and X. Dai[6]

[1]*Department of Condensed Matter Physics and Materials Science, Brookhaven National Laboratory, Upton, New York 11973, USA*

[2]*Materials Physics and Applications Division, Los Alamos National Laboratory, Los Alamos, New Mexico 87545, USA*

[3]*Condensed Matter Group, National High Magnetic Field Laboratory, Florida State University, Tallahassee, Florida 32310, USA*

[4]*Advanced Photon Source, Argonne National Laboratory, Argonne, Illinois 60439, USA*

[5]*School of Physical Sciences, Dublin City University, Dublin 9, Ireland*

[6]*Beijing National Laboratory for Condensed Matter Physics and Institute of Physics, Chinese Academy of Sciences, Beijing 100190, China*

[7]*Department of Physics and Astronomy, Rutgers University, Piscataway, New Jersey 08856, USA*

Resonant elastic x-ray scattering is a powerful technique for measuring multipolar order parameters. In this paper, we theoretically and experimentally study the possibility of using this technique to detect the proposed multipolar order parameters in URu$_2$Si$_2$ at the U-L_3 edge with the electric quadrupolar transition. Based on an atomic model, we calculate the azimuthal dependence of the quadrupolar transition at the U-L_3 edge. The results illustrate the potential of this technique for distinguishing different multipolar order parameters. We then perform experiments on ultraclean single crystals of URu$_2$Si$_2$ at the U-L_3 edge to search for the predicted signal, but do not detect any indications of multipolar moments within the experimental uncertainty. We theoretically estimate the orders of magnitude of the cross section and the expected count rate of the quadrupolar transition and compare them to the dipolar transitions at the U-M_4 and U-L_3 edges, clarifying the difficulty in detecting higher order multipolar order parameters in URu$_2$Si$_2$ in the current experimental setup.

I. INTRODUCTION

The heavy-fermion compound URu$_2$Si$_2$ undergoes a phase transition at $T_{HO} = 17.5$ K to the so-called "hidden order" (HO) phase, in which the sharp discontinuous specific heat signals a clear second-order phase transition [1]. Earlier studies based on neutron scattering [2,3] and muon spin rotation [4] conclude that it is a phase transition to a type-I antiferromagnet with the ordered moment polarized along the tetragonal c axis. However, the observed ordered moment is anomalously very small ($\sim 0.04 \pm 0.01 \mu_B$) [2–4], which cannot account for the observed large entropy loss ($\sim 0.2R \ln 2$), and the primary order parameter (OP) is unlikely to be a magnetic dipole. Further high-pressure experiments on URu$_2$Si$_2$ find a first-order phase transition from the HO phase to a large moment antiferromagnetic (LMAF) phase [5–7]. These findings further indicate that the HO phase is distinct from the LMAF and the primary OP should be some complex object which is different from a magnetic dipole.

Theoretically, many different schemes of OPs have been proposed, such as multipolar order [8–18], charge- or spin-density wave [19–22], chiral spin state [23], orbital antiferromagnetism [24], helicity order [25], dynamic symmetry breaking [26], nematic order [27], hybridization wave [28], and hastatic order [29,30]. However, through 30 years of efforts, there is still a lack of convincing evidence to uncover the HO mystery. For a more complete review of the theoretical and experimental progress, see Refs. [31,32].

Among the many proposals of OPs, the multipolar order is a promising candidate. Recently, Raman-scattering experiments [33–35] find a sharp low-energy excitation with A_{2g} symmetry below T_{HO}. Further analysis [34,35] indicates that this A_{2g} excitation is consistent with the hexadecapolar order proposed by Haule and Kotliar [14]. However, these Raman-scattering experiments provide indirect information about the ground state in the sense that they cannot measure modes at the ordering wave vector. Wave-vector-resolved techniques are desirable to make more definitive conclusions. Among the many options, resonant elastic x-ray scattering (REXS) is a powerful tool to directly detect the order of electrons including complex spin and charge multipoles [36,37]. There have been already a few REXS experiments [38–41] performed to identify the multipolar order in the HO phase of URu$_2$Si$_2$. Amitsuka *et al.* [40] and Walker *et al.* [41] performed REXS experiments at the U-M_4 ($3d_{3/2} \rightarrow 5f$) edge below T_{HO} and their results have excluded the possibility of any quadrupolar OPs. However, the M_4 edge involves electric dipolar transitions ($E1$) and has minimal sensitivity to multipoles with a rank larger than 2. The electric quadrupolar transition ($E2$) can be used to detect octupole and hexadecapole, but unfortunately, the intensity of $E2$ is usually much weaker than that of $E1$.

Recently, dos Reis *et al.* [42] discussed a sizable $E2$ contribution to the U-$L_{2,3}$ x-ray magnetic circular dichroism signal in their study of U compounds. The enhanced $E2$ signal may be due to the large wave vector k (10.615 and 8.699 Å^{-1}) at $L_{2,3}$ edges which means that the term $i\boldsymbol{k} \cdot \boldsymbol{r}$ in the expansion of $e^{i\boldsymbol{k} \cdot \boldsymbol{r}}$ cannot be ignored. This unexpected finding provides a promising hope to use the $E2$ transition to directly detect multipolar OPs in URu$_2$Si$_2$.

In this paper, we theoretically and experimentally study the possibility to detect the proposed multipolar OPs in URu$_2$Si$_2$ via $E2$ transition of REXS. Based on an atomic model, we first calculate the azimuthal dependences to show that it can identify different multipolar OPs by symmetry. Then, we do REXS experiments on an ultraclean sample of URu$_2$Si$_2$ single
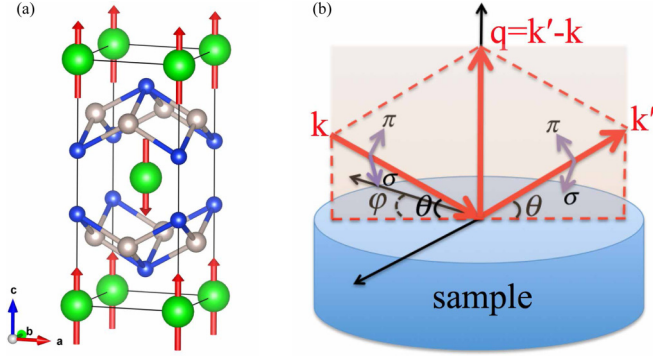
FIG. 1. (a) The crystal structure of URu$_2$Si$_2$. We assume a type-I antiferromultipolar order on uranium sites. (b) Illustration of experimental setup. A beam of polarized x rays k is incident on the [001] sample face with an angle θ and scattered by electrons, and then the scattered x rays k' with outgoing angle θ and specific polarization is analyzed. φ is the azimuthal angle. For linear polarization, π (σ) polarization is parallel (normal) to the scattering plane.

crystal to search for the possible signal of multipolar OPs. Finally, we justify the experimental results by theoretically estimating the relative strength of $E2$ transition at the L_3 edge (L_3-$E2$) compared with $E1$ transition at the M_4 edge (M_4-$E1$) and L_3 edge ($2p_{3/2} \rightarrow 6d$, L_3-$E1$), and the expected flux of the scattered photons.

II. METHODS

A. Atomic calculations

Figure 1(a) is the crystal structure of URu$_2$Si$_2$, which has a body-centered tetragonal structure. In the present study, we assume a type-I antiferromultipolar order on U sites, where sublattice A, U(0,0,0), and sublattice B, U(0.5,0.5,0.5), have opposite signs of the expectation value of the multipolar moment. The ordering wave vector is $Q_{AF} = (0,0,1)$. Figure 1(b) is a typical experimental setup of REXS. A beam of polarized x ray k is incident on the sample with an angle θ and then the scattered x ray k' with outgoing angle θ and specific polarization is analyzed. The double-differential cross section [36] for REXS is

$$\frac{d^2\sigma}{d\Omega\,dE} = r_e^2 m^2 \omega_{k'}^3 \omega_k |\mathcal{F}_{gg}(k,k',\hbar\omega_k,\hbar\omega_{k'},\epsilon,\epsilon')|^2, \quad (1)$$

where $r_e = e^2/(4\pi\epsilon_0 mc^2)$ is the classical electron radius, $\mathcal{F}_{gg}$ is the scattering amplitude at zero temperature,

$$\mathcal{F}_{gg}(k,k',\hbar\omega_k,\hbar\omega_{k'},\epsilon,\epsilon') = \sum_n \frac{\langle g \mid \hat{\mathcal{D}}'^\dagger \mid n \rangle \langle n \mid \hat{\mathcal{D}} \mid g \rangle}{\hbar\omega_k + E_g - E_n + i\Gamma/2}, \quad (2)$$

where k is the incoming light with energy $\hbar\omega_k$ and polarization ϵ, k' is the outgoing light with energy $\hbar\omega_{k'}$ and polarization ϵ', and $q = k' - k$ is the scattering vector. $\mid g \rangle$, E_g is the ground state and $\mid n \rangle$, E_n is the eigenstate of the intermediate Hamiltonian including a core hole. Γ is the lifetime width of the core hole. For U, $\Gamma \approx 8$ eV at the L_3 edge and $\Gamma \approx 3.5$ eV at the M_4 edge. $\hat{\mathcal{D}}$ and $\hat{\mathcal{D}}'^\dagger$ are the transition operators for

absorption and emission processes,

$$\hat{\mathcal{D}} = P^{(m)} \cdot \sum_R \hat{D}_R^{(m)} = P^{(m)} \cdot \left(\sum_R e^{ik\cdot R} \sum_i \hat{r}_{R,i}^{(m)} \right), \quad (3)$$

$$\hat{\mathcal{D}}'^\dagger = P^{(m)'\star} \cdot \sum_R \hat{D}_R^{(m)\dagger} = P^{(m)'\star} \cdot \left(\sum_R e^{-ik'\cdot R} \sum_i \hat{r}_{R,i}^{(m)\dagger} \right), \quad (4)$$

where R is the site index, and i is the index of electron that is bound to site R. $P^{(m)}$ is a rank-m tensor for the geometry part including polarization and wave vector of photon, $\hat{r}^{(m)}$ is a single-particle rank-m tensor operator of electron.

For the $E1$-$E1$ transition,

$$P^{(1)} \cdot \hat{r}^{(1)} = \epsilon_x \hat{x} + \epsilon_y \hat{y} + \epsilon_z \hat{z}, \quad (5)$$

$$P^{(1)'\star} \cdot \hat{r}^{(1)\dagger} = \epsilon_x'^\star \hat{x} + \epsilon_y'^\star \hat{y} + \epsilon_z'^\star \hat{z}. \quad (6)$$

For the $E2$-$E2$ transition [43],

$$(\hat{r}^{(2)})_1 = \frac{\sqrt{3}}{2}(\hat{x}^2 - \hat{y}^2), \quad (7)$$

$$(\hat{r}^{(2)})_2 = \tfrac{1}{2}(3\hat{z}^2 - \hat{r}^2), \quad (8)$$

$$(\hat{r}^{(2)})_3 = \sqrt{3}\hat{y}\hat{z}, \quad (9)$$

$$(\hat{r}^{(2)})_4 = \sqrt{3}\hat{z}\hat{x}, \quad (10)$$

$$(\hat{r}^{(2)})_5 = \sqrt{3}\hat{x}\hat{y}, \quad (11)$$

and

$$P_1^{(2)} = \frac{k}{3}\frac{\sqrt{3}}{2}(\epsilon_x \tilde{k}_x - \epsilon_y \tilde{k}_y), \quad (12)$$

$$P_2^{(2)} = \frac{k}{3}\frac{1}{2}(2\epsilon_z \tilde{k}_z - \epsilon_x \tilde{k}_x - \epsilon_y \tilde{k}_y), \quad (13)$$

$$P_3^{(2)} = \frac{k}{3}\frac{\sqrt{3}}{2}(\epsilon_y \tilde{k}_z + \epsilon_z \tilde{k}_y), \quad (14)$$

$$P_4^{(2)} = \frac{k}{3}\frac{\sqrt{3}}{2}(\epsilon_z \tilde{k}_x + \epsilon_x \tilde{k}_z), \quad (15)$$

$$P_5^{(2)} = \frac{k}{3}\frac{\sqrt{3}}{2}(\epsilon_x \tilde{k}_y + \epsilon_y \tilde{k}_x), \quad (16)$$

where k and $\tilde{k}$ are the length and direction of the wave vector, respectively. We assume the absorption and emission process take place at the same site, then the scattering amplitude can be written as

$$\mathcal{F}_{gg} \propto \sum_R e^{-iq\cdot R} F_{gg}^R, \quad (17)$$

with

$$F_{gg}^R = \sum_n \frac{\langle g \mid \hat{\mathcal{D}}_R^\dagger \mid n \rangle \langle n \mid \hat{\mathcal{D}}_R \mid g \rangle}{\hbar\omega_k + E_g - E_n + i\Gamma/2}, \quad (18)$$

where $\hat{\mathcal{D}}_R = P^{(m)} \cdot \hat{D}_R^{(m)}$ and $\hat{\mathcal{D}}_R^\dagger = P^{(m)'\star} \cdot \hat{D}_R^{(m)\dagger}$.

We further make a single-atom approximation, i.e., approximating the states $|g\rangle$ and $|n\rangle$ as single atomic states. Then the total scattering amplitude can be written as the summation of the contributions from two sublattices A and B of U atoms,

$$\mathcal{F}_{gg} \propto \sum_{\boldsymbol{R}_A} e^{-i\boldsymbol{q}\cdot\boldsymbol{R}_A} F_{gg}^{\boldsymbol{R}_A} + \sum_{\boldsymbol{R}_B} e^{-i\boldsymbol{q}\cdot\boldsymbol{R}_B} F_{gg}^{\boldsymbol{R}_B}, \qquad (19)$$

where

$$F_{gg}^{\boldsymbol{R}_A} = \sum_n \frac{\langle g^A | \hat{\mathcal{D}}_{\boldsymbol{R}_A}^{\dagger} | n^A\rangle\langle n^A | \hat{\mathcal{D}}_{\boldsymbol{R}_A} | g^A\rangle}{\hbar\omega_k + E_{g^A} - E_{n^A} + i\Gamma/2}, \qquad (20)$$

$$F_{gg}^{\boldsymbol{R}_B} = \sum_n \frac{\langle g^B | \hat{\mathcal{D}}_{\boldsymbol{R}_B}^{\dagger} | n^B\rangle\langle n^B | \hat{\mathcal{D}}_{\boldsymbol{R}_B} | g^B\rangle}{\hbar\omega_k + E_{g^B} - E_{n^B} + i\Gamma/2}. \qquad (21)$$

$|g^A\rangle(|n^A\rangle)$ and $|g^B\rangle(|n^B\rangle)$ are the ground (intermediate) states of U atoms A and B, respectively. In calculation, we choose the ground states to induce opposite signs of the expectation value of multipolar moment at the A and B sites.

We use the Cowan-Butler-Thole approach [44–47] to exactly diagonalize the atomic Hamiltonian for ground and excited configurations and then get the transition matrix. For URu$_2$Si$_2$, we assume a $5f^2$ ground configuration. For the M_4-$E1$, L_3-$E1$ and L_3-$E2$ transitions, the excited configurations are $3d^5 5f^3$, $2p^5 5f^2 6d^1$, and $2p^5 5f^3$, respectively. The Slater integrals F^k, G^k and spin-orbit coupling (SOC) ζ of the valence and core electrons are calculated by the Hartree-Fock (HF) methods in Cowan's code [44]. Usually, HF will overestimate them, so we rescale F^k, G^k by 80% and rescale SOC ζ by 92% for $2p$ core hole and 96% for $3d$ core hole, respectively. The parameters are listed in Tables I–IV in the Appendix.

According to Hund's rule coupling, the $5f^2$ configuration has a ground state with total angular momentum $J = 4$ under $SO(3)$ symmetry. With D_{4h} crystalline electric field symmetry, these nine ground states will split into five singlets and two doublets [17,48]:

$$\left|A_{1g}^{(1)}(\alpha)\right\rangle = \cos\alpha|0\rangle + \frac{\sin\alpha}{\sqrt{2}}(|4\rangle + |-4\rangle), \qquad (22)$$

$$\left|A_{1g}^{(2)}(\alpha)\right\rangle = \sin\alpha|0\rangle - \frac{\cos\alpha}{\sqrt{2}}(|4\rangle + |-4\rangle), \qquad (23)$$

$$|A_{2g}\rangle = \frac{i}{\sqrt{2}}(|4\rangle - |-4\rangle), \qquad (24)$$

$$|B_{1g}\rangle = \frac{1}{\sqrt{2}}(|2\rangle + |-2\rangle), \qquad (25)$$

$$|B_{2g}\rangle = \frac{i}{\sqrt{2}}(|2\rangle - |-2\rangle), \qquad (26)$$

$$\left|E_g^{(1)}(\beta)\right\rangle = \cos\beta|\mp 1\rangle + \sin\beta|\pm 3\rangle, \qquad (27)$$

$$\left|E_g^{(2)}(\beta)\right\rangle = \sin\beta|\mp 1\rangle - \cos\beta|\pm 3\rangle. \qquad (28)$$

In Ref. [17], the authors list the definition of the multipole up to rank 5. We will follow this definition in the present paper and only discuss multipole up to rank 4 that can, in principle, be detected via the $E2$ transition. We build different ground states which will induce dipole, quadrupole, octupole, and hexadecapole orders.

The ground state that will induce A_{2+} (A_{2-}) order can be constructed by a linear combination of $|A_{2g}\rangle$ and $|A_{1g}^{(2)}\rangle$,

$$|g^{A(B)}\rangle = \frac{1}{\sqrt{2}}\left(|A_{2g}\rangle \pm e^{i\eta}\left|A_{1g}^{(2)}(40^o)\right\rangle\right), \qquad (29)$$

where the plus sign is for $|g^A\rangle$ and the minus sign for $|g^B\rangle$. Note that the subscript $+$ $(-)$ in A_{2+} (A_{2-}) means time-reversal even (odd). When $\eta = 0$, it will induce a A_{2+} hexadecapolar order $H_z^{\alpha} = \frac{\sqrt{35}}{2}\overline{J_x J_y(J_x^2 - J_y^2)}$, while $\eta = \pi/2$ will induce a A_{2-} dipolar order J_z and octupolar order $T_z^{\alpha} = \frac{1}{2}\overline{J_z(5J_z^2 - 3J^2)}$. This scheme is proposed by Haule and Kotliar [14] by a LDA+DMFT calculation. In their LDA+DMFT calculation, they also figure out α in $A_{1g}^{(2)}$ should be about 40°. H_z^{α} is proposed to be the primary OP in the HO phase. It can be also induced as a secondary OP in the hastatic order scheme [30].

The ground state that will induce B_{1+} (B_{1-}) order can be written as

$$|g^{A(B)}\rangle = \frac{1}{\sqrt{2}}\left(|B_{1g}\rangle \pm e^{i\eta}\left|A_{1g}^{(2)}(40^o)\right\rangle\right). \qquad (30)$$

When $\eta = 0$, it will induce a B_{1+} quadrupolar order [10] $O_{22} = \frac{\sqrt{3}}{2}\overline{J_x^2 - J_y^2}$ and hexadecapolar order $O_{42} = \frac{\sqrt{5}}{4}\overline{(J_x^2 - J_y^2)(7J_z^2 - J^2)}$, while $\eta = \pi/2$ will induce a B_{1-} octupolar order [12] $T_{xyz} = \sqrt{15J_x J_y J_z}$.

The ground state that will induce B_{2+} (B_{2-}) order can be written as

$$|g^{A(B)}\rangle = \frac{1}{\sqrt{2}}\left(|B_{2g}\rangle \pm e^{i\eta}\left|A_{1g}^{(2)}(40^o)\right\rangle\right); \qquad (31)$$

when $\eta = 0$ it will induce a B_{2+} quadrupolar order [10] $O_{xy} = \sqrt{3J_x J_y}$ and hexadecapolar order $H_z^{\beta} = \frac{\sqrt{5}}{2}\overline{J_x J_y(7J_z^2 - J^2)}$, while $\eta = \pi/2$ will induce a B_{2-} octupolar order [12] $T_z^{\beta} = \frac{\sqrt{15}}{2}\overline{J_z(J_x^2 - J_y^2)}$.

B. REXS experiment

URu$_2$Si$_2$ samples were grown using the Czocharalski method [49]. The residual resistivity ratio (RRR) was measured in various pieces of sample; the REXS experiment was performed on the sample with the highest RRR ($=361$). REXS measurements were performed across the U-L_3 edge ($\approx$17.21 keV) at the 6-ID-B beamline of the Advanced Photon Source at Argonne National Laboratory. The sample was glued to a Cu holder using GE varnish. The holder was placed inside a Be dome filled with He gas, which in turn was mounted on the cold finger of a He closed cycle cryostat. A six circle diffractometer was used to move through reciprocal space. Measurements were performed using a scintillator point detector with 1×1 mm^2 slits. Tetragonal notation with $a = b = 4.108$ Å and $c = 9.514$ Å is used throughout the paper.
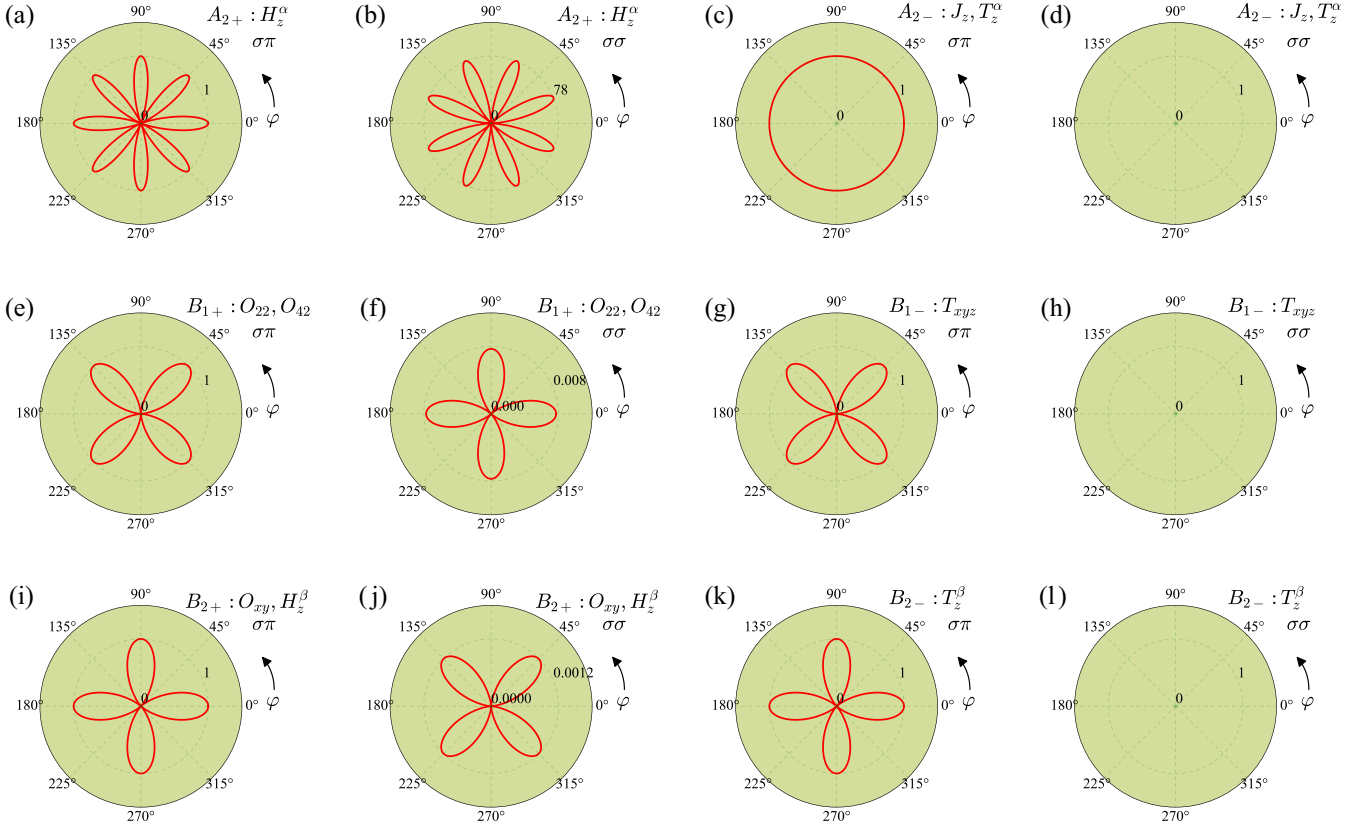
FIG. 2. The calculated azimuthal dependence of a (0,0,3) reflection of the L_3-$E2$ transition in both $\sigma\pi$ and $\sigma\sigma$ channels for different proposals of multipolar OPs. The incident photon energy is 17.167 keV and the azimuthal angle is defined with respect to the [100] direction. For each proposal, the intensity is normalized by the maximum intensity of its $\sigma\pi$ channel. (a),(b) A_{2+} hexadecapole H_z^α; (c),(d) A_{2-} dipole J_z and ocutpole T_z^α; (e),(f) B_{1+} quadrupole O_{22} and hexadecapole O_{42}; (g),(h) B_{1-} octupole T_{xyz}; (i),(j) B_{2+} quadrupole O_{xy} and hexadecapole H_z^β; (k),(l) B_{2-} octupole T_z^β.

III. RESULTS AND DISCUSSION

A. Azimuthal dependence for different multipolar order parameters

In REXS experiments, azimuthal measurements are used to identify the symmetry of the underlying OPs. Although Nagao *et al.* [43] have figured out the analytic formula of the azimuthal dependences for $E2$ transition, we still explicitly calculate and plot the azimuthal dependences to show the symmetry difference for different multipolar OPs. The results for a (0,0,3) reflection are plotted in Fig. 2. For each multipolar OP, both $\sigma\pi$ and $\sigma\sigma$ channels are plotted, and their intensity is normalized by the maximum of the $\sigma\pi$ channel. Figures 2(a) and 2(b) plot the results of the A_{2+} hexadecapole H_z^α. It shows an eightfold symmetry with a $\pi/8$ phase shift between the $\sigma\pi$ and $\sigma\sigma$ channels. The peak intensity of the $\sigma\sigma$ channel is about two orders of magnitude larger than that of the $\sigma\pi$ channel. The eightfold symmetry is a characteristic of this H_z^α hexadecapolar OP. Figures 2(c) and 2(d) show the results of the A_{2-} dipole J_z and octupole T_z^α. It shows a nonzero constant in the $\sigma\pi$ channel and no signal in the $\sigma\sigma$ channel. Figures 2(e) and 2(f) display the results of the B_{1+} quadrupole O_{22} and hexadecapole O_{42}. It shows a d_{xy} wave pattern in the $\sigma\pi$ channel and $d_{x^2-y^2}$ wave pattern in the $\sigma\sigma$ channel. In Figures 2(g) and 2(h) the results of the B_{1-} octupole T_{xyz}

shows a d_{xy} wave pattern in the $\sigma\pi$ channel and no signal in the $\sigma\sigma$ channel. Figures 2(i) and 2(j) plot the results of the B_{2+} quadrupole O_{xy} and hexadecapole H_z^β exhibiting a $d_{x^2-y^2}$ wave pattern in the $\sigma\pi$ channel and a d_{xy} pattern in the $\sigma\sigma$ channel. Finally, the results of the B_{2-} octupole T_z^β are shown in Figs. 2(k) and 2(l) where a $d_{x^2-y^2}$ wave pattern is seen in the $\sigma\pi$ channel and nothing is seen in the $\sigma\sigma$ channel. In general, we find that there are no signals in the $\sigma\sigma$ channel for time-reversal broken OPs. The azimuthal dependence shows different symmetries for different multipoles, so it can be used to distinguish multipolar OPs.

B. REXS results

The body-centered tetragonal structure of URu$_2$Si$_2$ forbids Bragg peaks with $H + K + L = 2n + 1$. We infer that the HO state breaks the body-centered symmetry by creating inequivalent U sites, thus allowing Bragg peaks at these once forbidden positions. We performed an extensive search for HO Bragg peaks along the (0,0,L) and (1,0,L) directions; results for the former are displayed in Fig. 3. Broad peaks are observed at $(0,0,2n + 1)$. However, these peaks persist through the phase transition at T_{HO}, strongly suggesting that these are not related to the HO phase. Additionally, no resonance enhancement is observed across the U-L_3 edge. This suggests
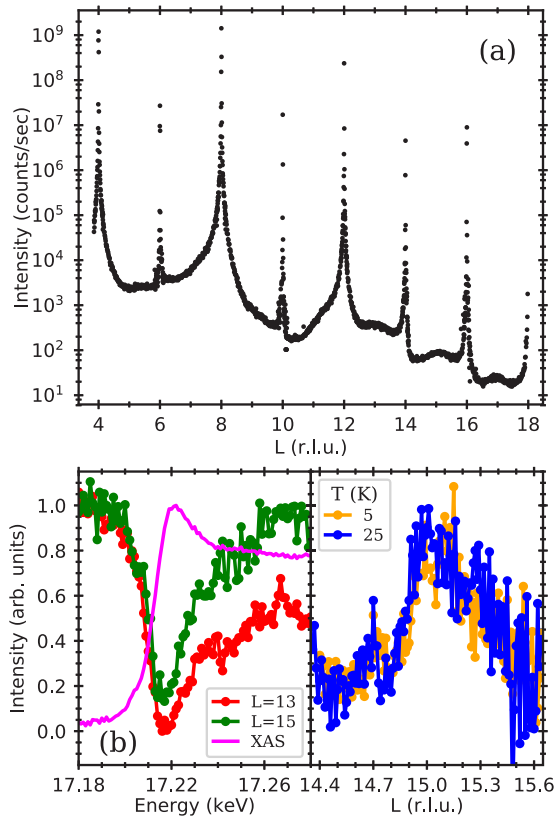
FIG. 3. (a) X-ray diffraction L dependence measured along the $(0,0,L)$ direction using 17.215 keV and $\varphi = 1.2°$. (b) Energy dependence of $(0,0,13)$ and $(0,0,15)$ Bragg peaks together with the U-L_3 edge XANES. (c) Temperature dependence of $(0,0,15)$ Bragg peak.

that the HO is not accessible through the $E1$ or $E2$ transitions using experiments of this type. These results are consistent with former studies [40,41] in which no quadrupolar OPs are found. However, we still cannot exclude the possibility of octupole and hexadecapole due to the weak signal of the $E2$ transition.

Despite our negative result in the search for the HO, additional experiments are needed to definitely prove the existence (or absence) of the octupole or hexadecapole OPs. Designing experimental techniques to enhance the sensitivity to the $E2$ transition at the U-L_3 edge is needed to observe higher rank multipoles. One such technique is the Borrmann spectroscopy [50,51]. The Borrmann effect refers to the anomalous transmission of x rays through very perfect single-crystal slabs when they are in symmetric Laue diffraction condition [50]. This effect can be interpreted by the theory of dynamical diffraction of x rays [50]. It is a consequence of multiple coherent interference of the incident and diffracted beams which produces a total electric field with almost zero amplitude but largely enhanced gradient at the crystal planes. The dipolar transition is thus suppressed because it is proportional to the amplitude of the electric field and, on the contrary, the quadrupolar transition will be largely enhanced because it is proportional to the gradient of the electric field. Therefore, we may have a chance to detect a strong quadrupolar signal, for example, at the U-L_3 edge. In Ref. [51], Pettifer

et al. indeed observed a very strong quadrupolar peak in the absorption spectrum at the L_1, L_2, and L_3 edges of gadolinium in a $4f$ compound gadolinium gallium garnet. However, no results of $5f$ compounds have been reported, so it is worth it to try in $5f$ compounds, such as URu$_2$Si$_2$. Borrmann spectroscopy requires samples that are much thicker than the nominal x-ray penetration depth and sufficiently perfect that at least some x rays can transmit through the sample without encountering defects, which may be a challenge for sample growth.

Polarization analysis of the outgoing x rays can also be advantageous (despite the strong reduction in x-ray throughput that it imposes) because, as we will demonstrate, the HO Bragg peak should be observed in the $\sigma\pi$ channel. Additionally, identifying the energy and cross section of the L_3-$E2$ transition will greatly facilitate the search for superlattice peaks.

C. Intensity estimation of the L_3-$E2$ transition

We further justify the negative experimental results by estimating the intensity of the L_3-$E2$ transition. Usually, the intensity of the $E2$ transition will be much weaker than that of the $E1$ transition. This is mainly caused by the very small overlap integral of r^2 between the core hole and valence orbitals. Thus, it is critical to give an estimation of the relative intensity of the L_3-$E2$ transition compared with known experiments which have strong intensity, such as the M_4-$E1$ transition. Roughly, the relative intensity between L_3-$E2$ and M_4-$E1$ is

$$\frac{I(L_3 - E2)}{I(M_4 - E1)} \propto \left(\frac{k}{3} \frac{\omega_{L_3}}{\omega_{M_4}} \frac{\langle 2p \,|\, r^2 \,|\, 5f \rangle}{\langle 3d \,|\, r \,|\, 5f \rangle} \right)^4 \left(\frac{\Gamma_{M_4}}{\Gamma_{L_3}} \right)^2, \quad (32)$$

and that between L_3-$E2$ and L_3-$E1$ is

$$\frac{I(L_3 - E2)}{I(L_3 - E1)} \propto \left(\frac{k}{3} \frac{\langle 2p \,|\, r^2 \,|\, 5f \rangle}{\langle 2p \,|\, r \,|\, 6d \rangle} \right)^4, \quad (33)$$

where ω_{L_3} and ω_{M_4} are the x-ray frequency of the L_3 and M_4 edges, and their ratio is about 4.6. Based on the HF calculations, the overlap integral ratios are $\langle 2p \,|\, r^2 \,|\, 5f \rangle / \langle 3d \,|\, r \,|\, 5f \rangle \approx 0.013$ and $\langle 2p \,|\, r^2 \,|\, 5f \rangle / \langle 2p \,|\, r \,|\, 6d \rangle \approx 0.2$, respectively. Γ_{M_4} and Γ_{L_3} are the core-hole lifetime widths for the M_4 and L_3 edges, respectively, and their ratio is $\Gamma_{M_4} / \Gamma_{L_3} \approx 0.4$. For the L_3 edge, $k/3 \approx 2.9$. Thus, the intensity of L_3-$E2$ is about 10^{-4} times smaller than that of M_4-$E1$ and 10^{-1} times smaller than that of L_3-$E1$. Here, we should note that $6d$ orbitals are much broader in URu$_2$Si$_2$, which will lead to larger overlap integrals than those based on the atomic $6d$ orbitals, so L_3-$E2$ is not just one order of magnitude smaller than that of L_3-$E1$. We may expect larger overlap integrals for the M_3-$E2$ ($3p_{3/2} \to 5f$) transition, so we also calculate the relative intensity between M_3-$E2$ and M_4-$E1$. The results show that the intensity of M_3-$E2$ is also about 10^{-4} times smaller than that of M_4-$E1$. The reason is that, although the calculated overlap integral $\langle 3p \,|\, r^2 \,|\, 5f \rangle$ is about 14 times larger than that of $\langle 2p \,|\, r^2 \,|\, 5f \rangle$, both the x-ray frequency and wave vector of the M_3 edge are about 0.25 times
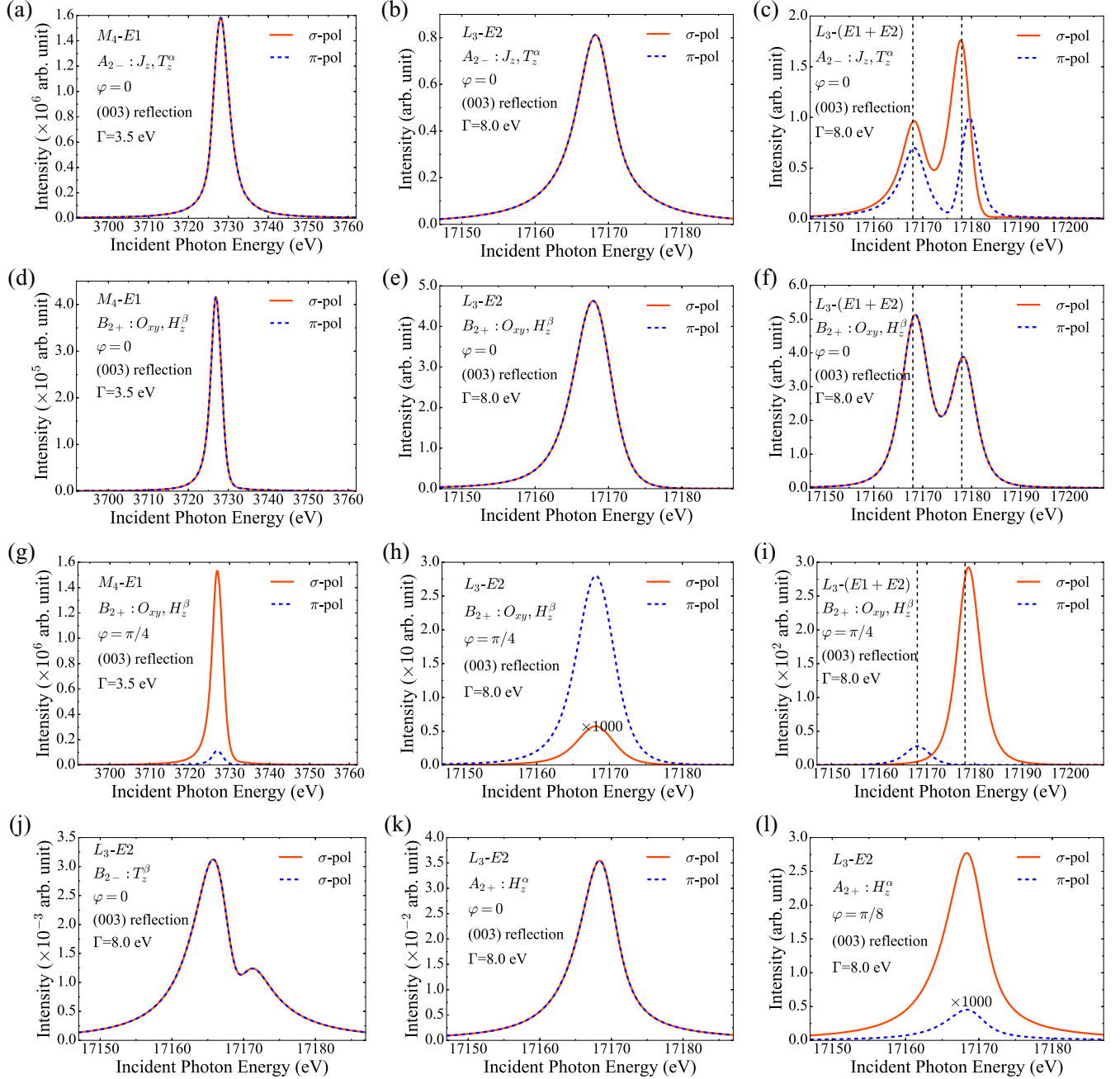
FIG. 4. (0,0,3) REXS intensity as a function of incident photon energy and polarization. The incoming light is linearly polarized and the polarization of the outgoing light is not analyzed. We compare the results of the M_4-$E1$ transition with the L_3-$E2$ transition and the L_3-$(E1 + E2)$ transition. We consider different ordering schemes: (a)–(c) Antiferrodipole J_z and antiferro-octupole T_z^α at $\varphi = 0$. (d)–(f) Antiferroquadrupole O_{xy} and antiferrohexadecapole H_z^β at $\varphi = 0$. (g)–(i) Antiferroquadrupole O_{xy} and antiferrohexadecapole H_z^β at $\varphi = \frac{\pi}{4}$. (j) Antiferro-octupole T_z^β at $\varphi = 0$. (k) Antiferrohexadecapole H_z^α at $\varphi = 0$. (l) Antiferrohexadecapole H_z^α at $\varphi = \pi/8$.

smaller than that of the L_3 edge; as a result, the enhancement effect from the larger overlap integral is canceled out. The intensity of M_3-$E2$ is not stronger than that of L_3-$E2$.

However, this rough estimation does not consider many details of the scattering process, such as the ground state and the intermediate excited states, the interference effects of intermediate states, the smearing effect of core-hole lifetime width, and the geometry of the experimental setup. To give a better estimation, we exactly diagonalize the atomic ground

and excited Hamiltonians to get the eigenstates and the transition matrix, and then we choose different ground states and experimental geometries to calculate the cross section according to Eqs. (1) and (2).

The calculated results of a (0,0,3) reflection are shown in Fig. 4. The azimuthal angle φ is defined with respect to the [100] direction and the polarization of outgoing light is not analyzed. We plot both the σ and π polarizations of the incident light. The difference of energy levels between $6d$ and $5f$ is

set to be 10 eV. We assume a type-I antiferromultipolar order with $Q_{AF} = (0,0,1)$ in the simulation. Figures 4(a)–4(c) are the results for the ground state [Eq. (29)] that induces A_{2-} orders: dipole J_z and octupole T_z^α. The $E1$ transition can only detect J_z but $E2$ can detect both of them. The azimuthal angle is set to be $\varphi = 0$. For this ground state, the intensity of L_3-$E2$ is about 10^{-6} times smaller than that of M_4-$E1$. However, the intensity of L_3-$E2$ is almost the same order of magnitude as that of the L_3-$E1$ transition. In Fig. 4(c), the left peak is from the $E2$ transition and the right peak is from the $E1$ transition. Figures 4(d)–4(i) plot the results for the ground state [Eq. (31)] that induces B_{2+} order: quadrupole O_{xy} and hexadecapole H_z^β. In Figs. 4(d)–4(f) the azimuthal angle is $\varphi = 0$. We find that the intensity of the L_3-$E2$ transition is 10^{-5} times smaller than that of the M_4-$E1$ transition and has the same order of magnitude as that of L_3-$E1$. In Figs. 4(g)–4(i), the azimuthal angle is set to be $\varphi = \pi/4$. For σ polarization, the intensity of L_3-$E2$ is about 10^{-9} times smaller than that of M_4-$E1$ and 10^{-5} smaller than that of L_3-$E1$. However, for π polarization, it is only 10^{-5} times smaller than that of M_4-$E1$ and much larger than that of L_3-$E1$ so that there is only an $E2$ peak. Figure 4(j) is the result for the ground state [Eq. (31)] that induces B_{2-} octupolar order T_z^β. The intensity is at least eight orders of magnitude smaller than that of M_4-$E1$. Another B_{1-} octupole T_{xyz} has the same order of magnitude as that of T_z^β. Figures 4(k) and 4(l) are the results for the ground state [Eq. (29)] that induces the A_{2+} hexadecapolar order H_z^α. For $\varphi = 0$, both σ and π polarizations are at least seven orders of magnitude smaller than that of M_4-$E1$. For $\varphi = \pi/8$, σ polarization is about five orders of magnitude smaller than that of M_4-$E1$. We emphasize that the atomic calculation underestimates the intensity of the L_3-$E1$ transition due to the itinerant character of $6d$ orbitals, so the intensity of L_3-$E1$ should be much larger than that of L_3-$E2$ in reality.

Based on these atomic results, we find that there are many factors that will affect the REXS cross section, such as the interference of the intermediate states, the interference effect of core-hole lifetime width, the experimental geometry, and the details of the ground states. Overall, the intensity of the L_3-$E2$ transition is at least five or six orders of magnitude smaller than that of M_4-$E1$, so the signal of the L_3-$E2$ transition is indeed very weak compared with M_4-$E1$. We also note that the $5f$ electrons are not completely localized and they have partial itinerant character in URu$_2$Si$_2$, which leads to the importance of the band effects in the REXS cross section. To account for these effects, the combination of more advanced first-principle calculations, such as density functional theory plus dynamical mean-field theory (DFT+DMFT), with REXS cross-section calculations is needed. Despite this, the simple atomic simulations still give us preliminary estimations about the strength of the $E2$ transition.

To further confirm the weakness of the L_3-$E2$ signal, we estimate the flux of the scattered photons by calculating the absolute value of the cross section. For a typical flux of 10^{11} ph/s/100 meV/(100×100 μm^2), a rough upper bound of the flux of scattered photons is 10^4 ph/s/eV/rad for the M_4-$E1$ transition, while it is 10^{-1}–10^{-2} ph/s/eV/rad for the L_3-$E2$ transition. This makes it very difficult to detect in experiments, which is consistent with the experimental results.

TABLE I. Slater integrals and spin-orbit coupling parameters for ground configuration $5f^2$ (in eV).

F_{ff}^0	F_{ff}^2	F_{ff}^4	F_{ff}^6	ζ_{5f}
0.291	7.611	4.979	3.655	0.261

IV. SUMMARY

In summary, we have studied the possibility to detect multipolar OPs in URu$_2$Si$_2$ by REXS in the U L_3-$E2$ transition channel. The REXS experiments do not find any clear signal indicating multipolar OPs. An estimation based on atomic calculations indicates that the intensity of the L_3-$E2$ transition is indeed much smaller than that of the M_4-$E1$ transition and the flux of the scattered photons is too small such that it is very difficult to detect the $E2$ signal. It seems that it is still not practical to use the $E2$ transition of currently available REXS experiments to detect the multipolar OPs. Developing experimental techniques to enhance the $E2$ signal is urgently needed to identify the multipolar OPs not only in URu$_2$Si$_2$ but also in other compounds, such as UO$_2$, NpO$_2$, and Ce$_{1-x}$La$_x$B$_6$ [52].

APPENDIX: SLATER INTEGRALS AND SPIN-ORBIT COUPLING PARAMETERS

We list the Slater integrals and spin-orbit coupling parameters used in our calculations in Tables I–IV.

TABLE II. Slater integrals and spin-orbit coupling parameters for excited configuration $2p^5 5f^3$ (in eV).

F_{ff}^0	F_{ff}^2	F_{ff}^4	F_{ff}^6	F_{pf}^0	F_{pf}^2	G_{pf}^2	G_{pf}^4
0.306	7.984	5.232	3.845	0.005	0.497	0.082	0.053
ζ_{5f}	ζ_{2p}						
0.302	2517.292						

TABLE III. Slater integrals and spin-orbit coupling parameters for excited configuration $2p^5 5f^2 6d^1$ (in eV).

F^0_{ff}	F^2_{ff}	F^4_{ff}	F^6_{ff}	F^0_{pf}	F^2_{pf}	G^2_{pf}	G^4_{pf}
0.307	8.278	5.447	4.011	0.102	0.528	0.087	0.056
F^0_{pd}	F^2_{pd}	G^1_{pd}	G^3_{pd}	F^0_{fd}	F^2_{fd}	F^4_{fd}	G^1_{fd}
0.022	0.272	0.238	0.142	0.139	3.750	2.050	1.938
G^3_{fd}	G^5_{fd}	ζ_{5f}	ζ_{6d}	ζ_{2p}			
1.562	1.213	0.321	0.435	2517.236			

TABLE IV. Slater integrals and spin-orbit coupling parameters for excited configuration $3d^5 5f^3$ (in eV).

F^0_{ff}	F^2_{ff}	F^4_{ff}	F^6_{ff}	F^0_{df}	F^2_{df}	F^4_{df}
0.307	8.020	5.258	3.865	0.102	2.051	0.952
G^1_{df}	G^3_{df}	G^5_{df}	ζ_{5f}	ζ_{3d}		
1.602	0.969	0.678	0.301	70.449		

[1] T. T. M. Palstra, A. A. Menovsky, J. van den Berg, A. J. Dirkmaat, P. H. Kes, G. J. Nieuwenhuys, and J. A. Mydosh, Phys. Rev. Lett. **55**, 2727 (1985).

[2] C. Broholm, J. K. Kjems, W. J. L. Buyers, P. Matthews, T. T. M. Palstra, A. A. Menovsky, and J. A. Mydosh, Phys. Rev. Lett. **58**, 1467 (1987).

[3] C. Broholm, H. Lin, P. T. Matthews, T. E. Mason, W. J. L. Buyers, M. F. Collins, A. A. Menovsky, J. A. Mydosh, and J. K. Kjems, Phys. Rev. B **43**, 12809 (1991).

[4] D. E. MacLaughlin, D. W. Cooke, R. H. Heffner, R. L. Hutson, M. W. McElfresh, M. E. Schillaci, H. D. Rempp, J. L. Smith, J. O. Willis, E. Zirngiebl, C. Boekema, R. L. Lichti, and J. Oostens, Phys. Rev. B **37**, 3153 (1988).

[5] H. Amitsuka, K. Matsuda, I. Kawasaki, K. Tenya, M. Yokoyama, C. Sekine, N. Tateiwa, T. Kobayashi, S. Kawarazaki, and H. Yoshizawa, J. Magn. Magn. Mater. **310**, 214 (2007).

[6] H. Amitsuka, M. Sato, N. Metoki, M. Yokoyama, K. Kuwahara, T. Sakakibara, H. Morimoto, S. Kawarazaki, Y. Miyako, and J. A. Mydosh, Phys. Rev. Lett. **83**, 5114 (1999).

[7] N. P. Butch, J. R. Jeffries, S. Chi, J. B. Leão, J. W. Lynn, and M. B. Maple, Phys. Rev. B **82**, 060408 (2010).

[8] P. Santini and G. Amoretti, Phys. Rev. Lett. **73**, 1027 (1994).

[9] P. Santini, Phys. Rev. B **57**, 5191 (1998).

[10] F. J. Ohkawa and H. Shimizu, J. Phys.: Condens. Matter **11**, L519 (1999).

[11] P. Santini, G. Amoretti, R. Caciuffo, F. Bourdarot, and B. Fåk, Phys. Rev. Lett. **85**, 654 (2000).

[12] A. Kiss and P. Fazekas, Phys. Rev. B **71**, 054415 (2005).

[13] K. Hanzawa, J. Phys.: Condens. Matter **19**, 072202 (2007).

[14] K. Haule and G. Kotliar, Nat. Phys. **5**, 796 (2009).

[15] F. Cricchio, F. Bultmark, O. Grånäs, and L. Nordström, Phys. Rev. Lett. **103**, 107202 (2009).

[16] H. Harima, K. Miyake, and J. Flouquet, J. Phys. Soc. Jpn. **79**, 033705 (2010).

[17] H. Kusunose and H. Harima, J. Phys. Soc. Jpn. **80**, 084702 (2011).

[18] H. Ikeda, M. Suzuki, R. Arita, T. Takimoto, T. Shibauchi, and Y. Matsuda, Nat. Phys. **8**, 528 (2012).

[19] M. B. Maple, J. W. Chen, Y. Dalichaouch, T. Kohara, C. Rossel, M. S. Torikachvili, M. W. McElfresh, and J. D. Thompson, Phys. Rev. Lett. **56**, 185 (1986).

[20] H. Ikeda and Y. Ohashi, Phys. Rev. Lett. **81**, 3723 (1998).

[21] V. P. Mineev and M. E. Zhitomirsky, Phys. Rev. B **72**, 014432 (2005).

[22] J. G. Rau and H.-Y. Kee, Phys. Rev. B **85**, 245112 (2012).

[23] L. P. Gor'kov and A. Sokol, Phys. Rev. Lett. **69**, 2586 (1992).

[24] P. Chandra, P. Coleman, J. A. Mydosh, and V. Tripathi, Nature (London) **417**, 831 (2002).

[25] C. M. Varma and L. Zhu, Phys. Rev. Lett. **96**, 036405 (2006).

[26] S. Elgazzar, J. Rusz, M. Amft, P. M. Oppeneer, and J. A. Mydosh, Nat. Mater. **8**, 337 (2009).

[27] S. Fujimoto, Phys. Rev. Lett. **106**, 196407 (2011).

[28] Y. Dubi and A. V. Balatsky, Phys. Rev. Lett. **106**, 086401 (2011).

[29] P. Chandra, P. Coleman, and R. Flint, Nature (London) **493**, 621 (2013).

[30] P. Chandra, P. Coleman, and R. Flint, Phys. Rev. B **91**, 205103 (2015).

[31] J. A. Mydosh and P. M. Oppeneer, Rev. Mod. Phys. **83**, 1301 (2011).

[32] J. Mydosh and P. Oppeneer, Philos. Mag. **94**, 3642 (2014).

[33] J. Buhot, M.-A. Méasson, Y. Gallais, M. Cazayous, A. Sacuto, G. Lapertot, and D. Aoki, Phys. Rev. Lett. **113**, 266405 (2014).

[34] H.-H. Kung, R. E. Baumbach, E. D. Bauer, V. K. Thorsmølle, W.-L. Zhang, K. Haule, J. A. Mydosh, and G. Blumberg, Science **347**, 1339 (2015).

[35] H.-H. Kung, S. Ran, N. Kanchanavatee, V. Krapivin, A. Lee, J. A. Mydosh, K. Haule, M. B. Maple, and G. Blumberg, Phys. Rev. Lett. **117**, 227601 (2016).

[36] L. J. P. Ament, M. van Veenendaal, T. P. Devereaux, J. P. Hill, and J. van den Brink, Rev. Mod. Phys. **83**, 705 (2011).

[37] T. Matsumura, H. Nakao, and Y. Murakami, J. Phys. Soc. Jpn. **82**, 021007 (2013).

[38] E. D. Isaacs, D. B. McWhan, R. N. Kleiman, D. J. Bishop, G. E. Ice, P. Zschack, B. D. Gaulin, T. E. Mason, J. D. Garrett, and W. J. L. Buyers, Phys. Rev. Lett. **65**, 3185 (1990).

[39] T. Nagao and J.-i. Igarashi, J. Phys. Soc. Jpn. **74**, 765 (2005).

[40] H. Amitsuka, T. Inami, M. Yokoyama, S. Takayama, Y. Ikeda, I. Kawasaki, Y. Homma, H. Hidaka, and T. Yanagisawa, J. Phys.: Conf. Ser. **200**, 012007 (2010).

[41] H. C. Walker, R. Caciuffo, D. Aoki, F. Bourdarot, G. H. Lander, and J. Flouquet, Phys. Rev. B **83**, 193102 (2011).

[42] R. D. dos Reis, L. S. I. Veiga, D. Haskel, J. C. Lang, Y. Joly, F. G. Gandra, and N. M. Souza-Neto, arXiv:1601.02443 (2016).

[43] T. Nagao and J.-i. Igarashi, Phys. Rev. B **74**, 104404 (2006).

[44] R. D. Cowan, *The Theory of Atomic Structure and Spectra* (University of California Press, Berkeley, 1981).

[45] P. H. Butler, *Point Group Symmetry Applications: Methods and Tables* (Plenum, New York, 1981).

[46] F. D. Groot and A. Kotani, *Core Level Spectroscopy of Solids* (CRC Press, Boca Raton, FL, 2008).

[47] E. Stavitski and F. M. de Groot, Micron **41**, 687 (2010).

[48] M. Sundermann, M. W. Haverkort, S. Agrestini, A. Al-Zein, M. Moretti Sala, Y. Huang, M. Golden, A. de Visser, P. Thalmeier, L. H. Tjeng, and A. Severing, Proc. Natl. Acad. Sci. USA **113**, 13989 (2016).

[49] T. D. Matsuda, D. Aoki, S. Ikeda, E. Yamamoto, Y. Haga, H. Ohkuni, R. Settai, and Y. Onuki, J. Phys. Soc. Jpn. **77**, 362 (2008).

[50] B. W. Batterman and H. Cole, Rev. Mod. Phys. **36**, 681 (1964).

[51] R. F. Pettifer, S. P. Collins, and D. Laundy, Nature (London) **454**, 196 (2008).

[52] P. Santini, S. Carretta, G. Amoretti, R. Caciuffo, N. Magnani, and G. H. Lander, Rev. Mod. Phys. **81**, 807 (2009).